Title

Free-standing and bendable carbon nanotubes/TiO2 nanofibres composite electrodes for flexible lithium ion batteries

Authors

Zhang, Peng
Qiu, Jingxia
Zheng, Zhanfeng
et al.

Publication Date

2013-08-01

DOI

10.1016/j.electacta.2013.04.089

Peer reviewed

Free-standing carbon nanotubes/TiO_2 nanofibers composite electrodes for flexible lithium ion batteries

Carbon nanotube (CNT) and TiO_2 nanofibre composite films are prepared for application in lithium ion batteries (LIBs). The preliminary experimental results from X-ray diffraction, scanning electron microscopy and transition electron microscopy suggest that the TiO_2 nanofibres were well-dispersed and interwoven by the CNTs, forming freestanding, bendable and light weighted composite. In comparison with TiO_2 nanofibre based LIBs, the CNTs significantly could improve the battery performance due to their high conductivity and 3-D network morphology. In both 1~3V and 0.01~3V testing voltage ranges, the as-prepared composites show excellent reversible capacity and capacity retention. The superior lithium storage property of CNT/TiO_2 composite was mainly attributed to due functions of the CNTs - the CNTs provide conductive networks to improve the electron transfer but also prevent agglomeration of TiO_2 nanofibres and facilitate lithium ion diffusion between the electrolyte and TiO_2 nanofibre active materials. This work suggests that the CNT-TiO_2 composite film could be the potential electrode material for large-scale LIB applications.

Introduction

Invention and development of wearable devices, portable electronic gadgets and rollup displays demands corresponding advance of safe, flexible, and light-weight power sources with high energy and power density.[1, 2] Due to the highest power density among all commercial secondary power sources, lithium ion batteries (LIBs) have been widely applied in portable devices since 1990s.[3] However, the conventional LIBs assembly processes cannot meet these needs without obtaining bendable and highly efficient electrodes. Typically, copper and aluminium have been used as the current collectors in LIBs due to their high conductivity and satisfactory mechanical strength. However, the energy and power density are limited by its two-dimensional electron collection manner and bending of the electrodes will damages the contact between active materials and current collectors.[2, 4] Furthermore, the use of binder in the conventional LIBs assembly will increase the assembly cost, produce organic solvent wastes and decrease the specific lithium ion storage.[5]

Fabrication of the free-standing electrode by incorporation of the active materials with carbonaceous nanomaterials such as carbon nanotubes or graphene is a promising way to address these issues in that it is flexible, highly conductive and its nanostructured framework can facilitate three-dimensional electron collection and enhance mass transport of lithium ions.[6-8] This approach has been applied to fabrication of both flexible cathodes such as V_2O_5/CNT, and anodes, such as, SnO_2/CNT, Silicon/graphene, and Co_3O_4/rGO/CNTs.[7-11] In a typical process, pre-treatment, such as flux or hydrothermal, is required to enhance the interaction between carbonaceous nanomaterials and active materials.[12, 13]

TiO_2 is a promising anode material for lithium ion batteries with a good cycling performance and can be charge/discharge at high current density due to its low volume expansion upon lithiation. Despite the different polymorphs, the most electrochemical active anatase delivers ca.167 mAh/g of capacity at ca. 1.75V (*vs.* Li/Li^+).[14] This process is corresponding to the lithium insertion/extraction in TiO_2 lattice which can be expressed by Eqn. 1:.[15]

$$xLi^+ + TiO_2 + xe^- \rightleftharpoons Li_xTiO_2 \qquad (1)$$

Recently, TiO_2 nanofiber was synthesized using hydrothermal method for photocatalyst application and showed high photocatalytic activity due to its one dimensional morphology which enhance charge transport along the longitudinal dimension and low electron-hole recombination rate.[16, 17] The adoption of TiO_2 nanofibres might utilise its large surface area and enhance lithium ion mass transport within the structure, subsequently, improve lithium storage capacity and rate capability. However, the low electronic conductivity of among the TiO_2 nanofibres limits its application in LIB commercialisation. The incorporation of the TiO_2 fibres into the CNTs 3-D networks will result in mechanically strong composites film, in which 3-dimensional electron collection can be achieved due to the high conductivity and flexibility of the CNTs.[18, 19] Moreover, the porosity of the composite film also could provide large contact area between TiO_2 active material and electrolyte and benefit the lithium diffusion. Therefore, it is envisaged that incorporation of CNTs and TiO_2 nanofibres could favour the transferring of the electrons and simultaneously the diffusion of lithium ions during charging and discharging in LIBs. Furthermore, the CNTs prevent nanostructured TiO_2 from agglomerating and maintain the lithium ion transport pathway between electrolyte and electrode. Additionally, binder-free electrodes have lightweight and flexible geometry for soft and bendable pack or alternative forms of batteries and can be operated at high temperature (even at 200ºC) at which the binder is not stable.[20]

[a] *Centre for Clean Environment and Energy, Environmental Futures Centre, and Griffith School of Environment, Gold Coast Campus, Griffith University QLD 4222, Australia.; E-mail: s.zhang@griffith.edu.au*

[b] *Inorganic Materials Research Program, School of Physical and Chemical Sciences, Queensland University of Technology, GPO Box 2434, Brisbane, QLD 4001, Australia.*

[c] *Environmental Energy Technologies Division and Advanced Light Source, Lawrence Berkeley National Laboratory, Berkeley, California 94720, USA.*

[d] *Discipline of Nanotechnology and Molecular Science, Queensland University of Technology, GPO Box 2434, Brisbane, QLD 4001,Australia.*

In this work, titanate nanofibres were firstly prepared via hydrothermal reaction and treated with HCl. The acid-treated titanate nanofibres were then calcined and turned into TiO_2 nanofibres.[16] The as-prepared TiO_2 nanofibres were evenly dispersed into an ultra-long CNT conductive network by prolonged ultrasonication. A free-standing and bendable membrane was obtained after the mixture is filtered through a filtration device. To our best knowledge, this is for the first time freestanding and flexible CNT/TiO_2 composite films are fabricated and studied for LIBs.

Experimental

TiO_2 nanofibers were synthesized using our method.[16] Briefly, anatase particles in 10M NaOH solution were treated in hydrothermal process at 180 ºC for 48 hours. After being washed by distilled water and exchanged with H^+ by diluted HCl, the dried solids was annealed at 700 ºC in air for 4 hours to obtain the TiO_2 nanofibers Multi-wall carbon nanotubes (CNTs) were functionalized by refluxing in concentrated HNO_3 and H_2SO_4 (1:3 volume ratio) at 130 ºC in an oil bath. The treated CNTs were then washed by DI-water to neutral and dried in vacuum oven at 60ºC. Under ultrasonication, the CNTs and TiO_2 nanofibers were dispersed evenly in distilled water and Triton X100 solution in weight ratio (pure carbon nanotubes to TiO_2 nanofibers) of 1:1 and 1:3 respectively (denoted as CT-1, and CT-3 respectively). After being ultrasonicated for 20 minutes, the solution was then filtered using a polyvinylidene difluoride (PVDF) membrane with a 0.1 μm pore size (Millipore, 47mm diameter), and then dried at 50 ºC.[6, 21]

The as-prepared CNT/TiO_2 composites were examined using field-emission scanning electron microscopy (FESEM, JEOS 7001) and high resolution transmission electron microscopy (HRTEM, JEM-2010). XRD patterns were obtained on X-ray diffraction (XRD, LabX-6000, Shimadzu, Japan) using Cu *Ká* radiation at 40 kV and 40 mA over a 2θ range of 10-80 °. Thermo-gravimetric analysis (TGA) was conducted between room temperature to 1000ºC in air.

The free-standing films were cut to 10.0×10.0mm pieces and assembled into CR2032 coin cells in an argon filled glove box (MBraun). In these cells, battery-grade lithium foils were acted as the counter electrode, and a 1M $LiPF_6$ in ethylene carbonate and dimethyl carbonate (EC:DMC, 1:1 ratio) was the electrolyte. Galvanostatic charge/discharge was carried out in the ranges of 0.01V to 3.0V and 1.0V to 3.0V *vs*. Li/Li^+ reference using LAND-CT2001A cycling testers (Wuhan, China). Cyclic voltammograms (CV) and electrochemical impedance spectroscopy (EIS) were performed using a CHI 660D electrochemical workstation (CH Instrument, China). CV was recorded between 3.0-1.0 V and 3.0-0.01V at a scan rate of 0.5mV/s. AC impendence spectra were carried out with amplitude of 5 mV over the frequency range from 100 kHz to 0.01 Hz.

Results and Discussion

Materials characterisation

The freestanding CNT, CT-1 and CT-3 thin films were obtained after the filtration process of the corresponding colloid solution after ultrasonic treatment. The CNT film was black colour, while CT-1 and CT-3 films were dark grey. The morphology of the TiO_2 nanofibres, CNTs and the as-prepared free-standing CNT/TiO_2 composite films were investigated by the FESEM and TEM. Under the SEM, it can be observed that most of TiO_2 nanofibres aggregated in parallel leading to significantly larger size in diameter, leading to the loss of one-dimensional property. Only a small portion of the TiO_2 nanofibres were. Most of the TiO_2 nanofibres have a diameter of 50-100nm and a length of 5 to 10 μm (Figure 1a). The TEM image (Figure 1b) shows that TiO_2 nanofibres grew along the [010] direction with a distance of 0.35nm between (011) facets (Figure 1b).[16] Figure 1c shows that CNTs were less than 50nm in diameter and ca. 1-5 μm in length. The CNTs were loosely interlinked with each other without the obvious agglomeration. After the sonication and filtration processes, the TiO_2 fibres were dispersed into the conductive CNT networks with different CNT/TiO_2 ratios (CT-1 in Figure 1d, CT-3 in Figure 1e,). The dark grey free-standing CT-1 film was flexible under a bending force as shown in insert of Figure 1d. The thickness of the film is about 10μm. Figure 1e shows that some TiO_2 fibres still agglomerated because of higher ratio of TiO_2 fibre in CT-3 sample. The diffraction patterns of the TiO_2 nanofibres and the composites in Figure 1f match the tetragonal anatase (JCPDS 21-1272, space group $I4_1/amd$) with the *d* value of 3.495Å for facet (011), which is consistent with the result of HRTEM in Figure 1b. This confirms that the TiO_2 nanofibre consists of pure anatase phase. Only a diffraction peak was observed at ca. 25° for (002) facet of the carbon nanotubes, which suggests that the carbon nanotube samples are of high purity. For CT-1 and CT-3 samples, all the diffraction peaks of the anatase were observed with attenuated intensity, while the (101) peak of anatase at 25° overlapped the (002) peak of carbon nanotube.[22] Figure 2 is the results of thermo-gravimetric analysis (TGA) in air. The TGA curves show that the major weight loss is occurred between 500 to 600ºC in all three samples, and after 600ºC the weight of samples are stable. Since TiO_2 is stable at this temperature range, the weight loss is corresponding to the loss of carbon nanotubes. Therefore, the weight percentages of TiO_2 in the as-prepared composites were 52.95% in CT-1, and 73.71% in CT-3 according to the weight differences before and after the oxidation of carbon nanotubes in air. This was consistent with 1:1 and 1:3 CNT/TiO_2 ratios in our sample preparation, respectively.

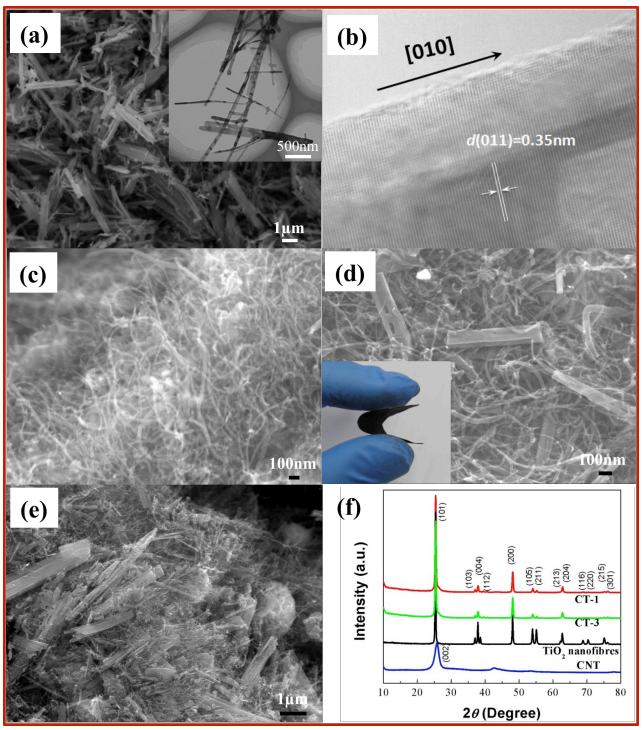

Figure 1 Materials characterisation of the as-prepared thin films: SEM (a) and HRTEM (b) images of the TiO_2 nanofibre, SEM images of the multi-wall CNTs (c), the free-standing CT-1 composites: (d), photograph of the bended CT-1 film (inset of d), and CT-3 (e), and XRD patterns (f).

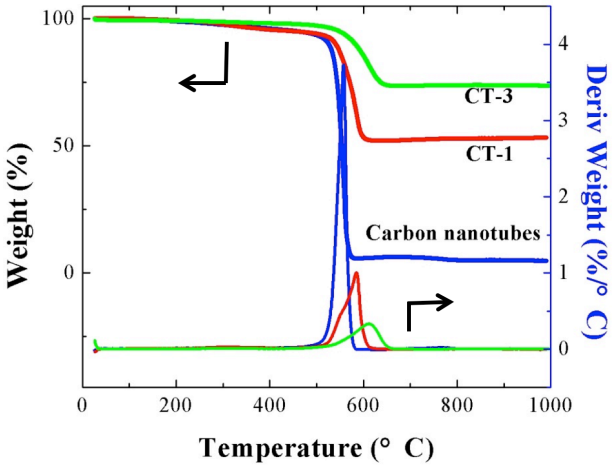

Figure 2 TGA profiles of the CNTs, CT-1 and CT-3.

LIB performance

Because CNTs have lithium ion storage capacity, the specific capacities for CT-1 and CT-3 are calculated based on the weight of TiO_2 after the deduction of the capacity contributed by CNTs in this work. In 1-3V voltage range, the discharging capacities were found to be 40mAh/g at initial cycle and 20mAh/g after 2nd cycle.

The galvanostatic charging/discharging tests at current density of 0.1C (16.7mA/g) for TiO_2 nanofibres, CT-1, CT-3 and pure CNTs within voltage range 1~3V (*vs.* Li/Li^+) were conducted as shown in Fig. 3. Figure 3a demonstrated that the CNT networks are effective in improving Li ion storage capacity and enhancing the cycling stability of TiO_2 nanofibres. In particular, at 0.1C current density, CT-1 showed 200mAh/g of discharging capacity at the initial cycle and about 150mAh/g of reversible capacity up to 100 cycles, while CT-3 exhibited 135mAh/g at the 1st cycle and about 125mAh/g after second cycle. In strong contrast, the pure TiO_2 nanofibres presented sharp capacity decays in the first 20 cycles (i.e. from above 200mAh/g at the initial cycle to about 25mAh/g after 20th cycle).

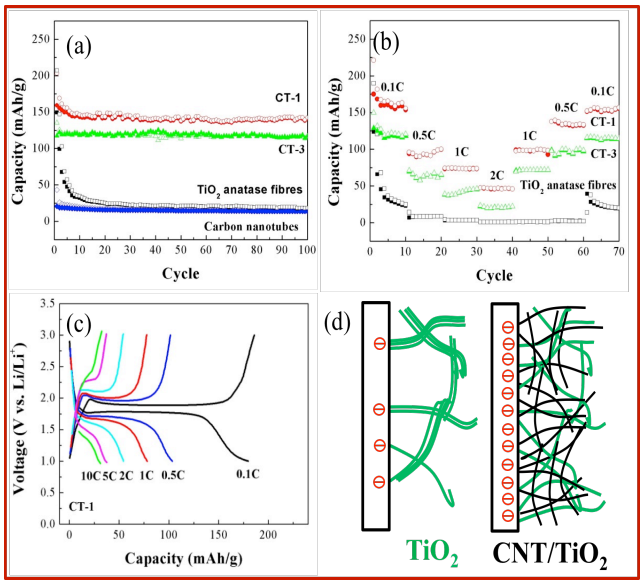

Figure 3 Galvanostatic tests of as-prepared CNT/TiO_2 composites (CT-1, CT-3, and TiO_2 nanofibres, carbon nanotubes) at 0.1C current density between 1-3V (vs. Li/Li+) (●▲■♦, Charge; ○Δ□◊, Discharge) (a), multi-current density galvanostatic tests of as-prepared CNT/TiO_2 composites (CT-1, CT-3, and TiO_2 nanofibres) at 0.1C-2C between 1-3V (●▲■, Charge; ○Δ□, Discharge) (b), charge/discharge profile of as-prepared CT-1 at multi-current density between 1-3V (c), Schematic drawing of TiO_2 nanofibre networks and as-prepared CNT/TiO_2 networks (d).

Figure 3b indicates that CT-1 and CT-3 possessed much higher rate capacity than the pure anatase nanofibres at the same C rate. Furthermore, the composite with higher CNT ratio (i.e., CT-1) showed higher capacity than the one with lower CNTs (CT-3), especially at higher current density. The excellent rate capability was achieved by CT-1 only, it delivered about 25mAh/g at both 5C rate (835mA/g) and 10C rate (1670 mA/g) (Figure 3c and 3d). In contrast, at 5C and 10C rates, the lithium storage capacities for CT-3 and the pure anatase nanofibres are practically negligible.

The relatively low efficiency of the TiO_2 nanofibres sample was likely due to two factors, i.e., the high temperature treatment of the fibres at 700ºC during the synthesis and the aggregation of the TiO_2 nanofibres in the electrode preparation. The former is harmful to electronic conductivity while the latter results in the dramatic loss of surface area of one-dimension nanofibre and therefore lithium ion diffusion efficiency (see schematic agglomeration representation in green colour in Fig 3d).[16, 23] The

incorporation of the CNT via the simple filtration process resulted in the formation of 3-dimensional CNT network, which has dual functions to simultaneously address these two problems. Firstly, the CNT network could provide efficient electron transport network, eliminate the low conductivity drawback of the TiO_2 nanofibres and therefore facilitate 3-D current collection as shown in Figure 3d. Secondly, the CNT networks not only maintain rapid mass transport characteristics of one-dimension nanofibres by preventing the TiO_2 nanofibres from agglomeration and providing porous network for high rate lithium ion diffusion.

EIS Kinetic Analysis

In order to verify the above hypothesis and clarify the relationship between CNT ratio and electrochemical kinetics, EIS measurement was carried out, because EIS is an efficient method to analyse the diffusion phenomena in the electronic and ionic mixed conductors (Figure 4a).[24] The EIS was conducted after 20 cycles and were discharged to a fixed depth of discharge, e.g., 0.2 Li for CT-1 and CT-3, 0.03 Li for TiO_2 nanofibres (Figure 4c). Figure 4a shows the Nyquist plots with a frequency range of 10^5-10^{-2}Hz for CT-1, CT-3 and TiO_2 nanofibres, respectively. It is well-established that the Nyquist plot at high frequency related to the overall internal resistance which represents the electrolyte resistance (R_s), and the charge-transfer resistance (R_{ct}). R_{ct} attribute to the lithium ion interfacial transfer.[24] R_s and R_{ct} of the samples were calculated using the equivalent circuit in Figure 4a and listed in table 1. There were only trivial differences (within a few Ohms) of the electrolyte resistances for all three samples due to the use of identical electrolyte systems. Compared with R_{ct} of the pristine TiO_2 nanofibres (214.3Ω), the R_{ct} of CT-1 and CT-3 have been reduced significantly to 38.99 Ω and 117.9 Ω respectively. This suggests that the CNTs can significantly improve conductivity of the electrode. Furthermore, the fact that higher CNTs contents (CT-1) resulted in larger conductivity than lower one (CT-3) confirms that the CNT networks could provide more pathways for charge transferring (Figure 3d).

Additionally, the linear *Warburg* regions at low frequency in Nyquist plots can be used to represent the lithium ion diffusion behaviour within the solid-state electrode materials.[24] In fact, the lithium ion diffusion coefficient can be quantified using the data in this region and equation (2):

$$D_{Li} = \frac{1}{2}\left[\left(\frac{Vm}{FA\sigma_w}\right)\frac{dE}{dx}\right]^2 \qquad (2)$$

where V_m is the molar volume of TiO_2 anatase (20.54 cm^3/mol), F is the Faraday constant, A is the total contact surface area between the electrolyte and the electrode, and σ_w is the *Warburg* prefactor obtaining from the *Warburg* region of impedance response.[24] The value of σ_w is determined by the slope of Z_{Re} vs. $\omega^{-1/2}$ at *Warburg* region (Figure 4b), which ω is the angular frequency.

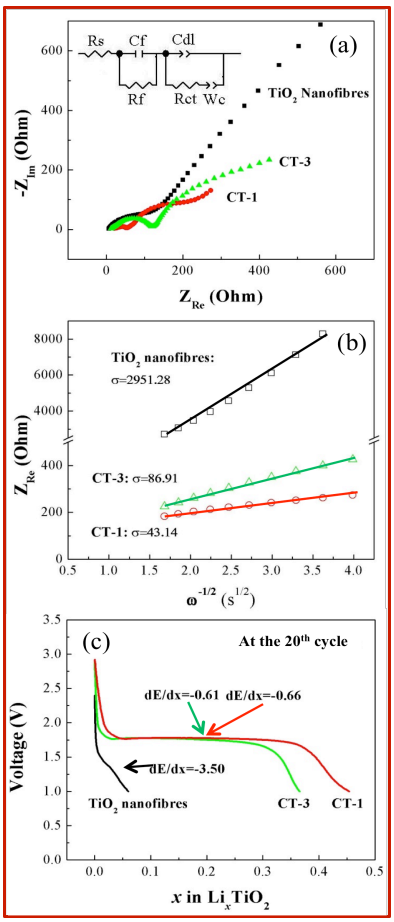

Figure 4 Nyquist plots and the equivalent circuit for CT-1, CT-3 and the TiO_2 nanofibres at specific depth of discharge (a); Z_{Re} *vs.* $\omega^{-1/2}$ plots in the low frequency region (b); discharge curves of CT-1, CT-3 and TiO_2 nanofibres which show the specific depth of discharge to calculate the lithium diffusion coefficient D_{Li} (c).

In order to obtain the value of *dE/dx*, the charge-discharge profile was plotted by converting the capacity into number of intercalated lithium ion, x at the 20th cycle in Figure 4c. Two discharging plateaus were observed for both CT-3 and CT-3 samples, indicating highly reversible lithium ion insertion capacity of the composite samples. In strong contrast, the TiO_2 nanofibres sample only showed a short slop instead of the typical discharging plateau, which suggests that the capacity of lithium insertion decayed dramatically at the 20th cycle. This may attribute to the severe agglomeration of nanofibres and subsequent considerable decrease of electrode/electrolyte contact area. Nevertheless, *dE/dx* was calculated by the slope of discharge curves at the depth of discharge as shown in Figure 4c.

Consequently, the lithium ion diffusion coefficients of samples were computed using equation (2) and summarised in Table 1. The D_{Li} of CT-1 and CT-3 samples are 6.02×10^{-17} and 4.69×10^{-17}, substantially larger (i.e., 60 and 40 times) than that of pristine TiO_2 nanofibers, respectively. These results support our hypothesis that the CNT network can improve the lithium ion diffusion within TiO_2 nanofibre networks by preventing TiO_2 nanofibres from agglomeration as proposed in Figure 3d.

Table 1 The lithium ion diffusion coefficient in CT-1, CT-3 and TiO2 nanofibres LIBs

	CNT/TiO_2 Ratio	D_{Li} (EIS) ($cm^2 \cdot s^{-1}$)	R_s	R_{ct}
CT-1	1:1	6.02×10^{-17}	11.09	38.99
CT-3	1:3	4.69×10^{-17}	14.36	117.9
TiO_2 nanofibres	0	1.01×10^{-18}	15.93	214.3

Expended working voltage range

The CV tests for the first 5 cycles of as-prepared CT-1within the potential window of 1-3V and 0.01-3V (*vs*. Li/Li^+) are shown in Figure 5a and 5b respectively. In Figure 5a, a pair of redox peaks at 1.65V and 2.15V (*vs*. Li/Li^+) are observed during the negative-scan and positive-scan, corresponding to the lithium insertion and lithium extraction reaction of anatase, respectively. The CV curves were stable and well overlapped each other after the second cycle, indicating the excellent reversibility and capacity retention of the as-prepared composite films. When the sweeping potential window is extended to 0.01V, a couple of redox peaks at ca.0.01V are observed which is corresponding to the lithium insertion/extraction of carbon (Figure 5b). The broad peak at about 0.4V at the first cycle of CV can be attributed to the irreversible capacity which is related to the decomposition of electrolyte and formation of solid-electrolyte interface (SEI). From the second cycle, the reduction peak at 0.4V is eliminated and all other redox peaks at about 0.01V, 1.65V and 2.15V are stable and not shifting, which indicates that the SEI film can prevent further decomposition of electrolyte and the as-prepared material has a high reversibility at the extended potential window. Figure 5c shows the cycling performance of CT-1 at the current density of 27mA/g between 0.01-3.0V. The initial capacity is over 700mAh/g with the columbic efficiency of 37%. After 5 cycles the capacity is over 220mAh/g and remained stable after 60 cycles. Figure 5d is the profile of CT-1 cycling between 0.01 and 3.0V at 2^{nd}, 10^{th} and 50^{th} cycle. The voltage plateaus at about 1.65V and 2.15V correspond to the lithium insertion and extraction reaction with TiO_2, while the slops close to 0.01V are related to the lithium insertion and extraction with tehe CNTs. The results of galvanostatic tests suggested that the composite not only possessed the improved electrochemical performance between 1-3V, but also can provide an extended and stable reversible capacity at 0.01-3V range. In other words, when the electrodes were discharged to below 1V, i.e., in 0.01-1V range, the carbon nanotubes were acting as the conductive network as well as the lithium ion hosts.

Conclusion

Flexible and free-standing CNT and TiO_2 nanofibre composite film has been prepared by the flow-directed flow assembly method. The as-prepared composite film can be used to as anode material for LIBs without the use of binders and conventional copper current collector. The CNTs are able to only provide conductive networks to improve the electron transfer but also prevented agglomeration of TiO_2 nanofibres and enhanced lithium ion conductivity between the electrolyte and TiO_2 nanofibre active materials. Consequently, the CNT/TiO_2 composite films demonstrated remarkable electrochemical performance in term of reversible capacity and rate capability in both 1-3V and 0.01-3V potential ranges. This work suggests that the free-standing CNT/TiO_2 composite film is a potential anode material for large-scale LIB application.

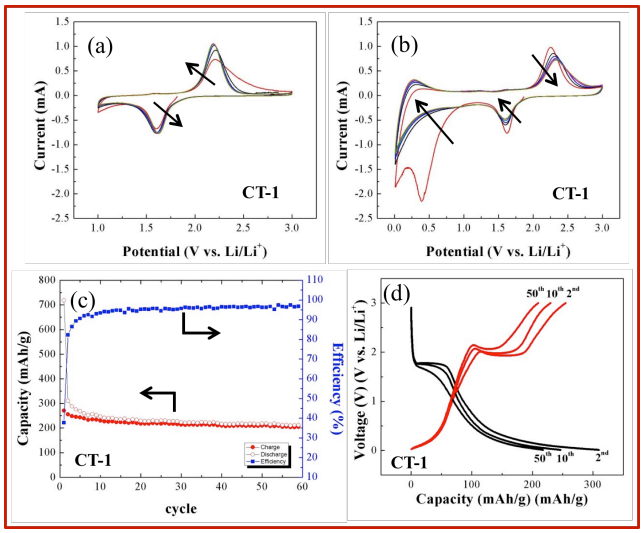

Figure 5 CV tests for the first 5 cycles of the as-prepared CT-1 within the potential window of 1-3V (a), and 0.01-3V (b), Galvanostatic tests (c) and charge/discharge profile (d) of as-prepared CT-1 at current density of 0.1C within the potential window of 0.01-3V. (We shall specifically workout the capacity of the same electrode (CT-1) in difference potential range).

Acknowledgement

The authors acknowledge the facilities and the scientific and technical assistance of the Australian Microscopy & Microanalysis Research Facility at the Centre for Microscopy and Microanalysis at The University of Queensland.

References

1 L. Hu, H. Wu, F. La Mantia, Y. Yang and Y. Cui, *ACS Nano*, 2010, **4**(10), 5843-5848.

2 H. Nishide and K. Oyaizu, *Science*, 2008, **319**(5864), 737-738.

3 B. Scrosati, J. Hassoun and Y.-K. Sun, *Energy Environ. Sci.*, 2011, **4**(9).

4 T. Marks, S. Trussler, A. J. Smith, D. J. Xiong and J. R. Dahn, *J. Electrochem. Soc.*, 2011, **158**(1), A51-A57.

5 N. Singh, C. Galande, A. Miranda, A. Mathkar, W. Gao, A. L. M. Reddy, A. Vlad and P. M. Ajayan, *Scientific Reports*, 2012, **2**, 481.

6 S. H. Ng, J. Wang, Z. P. Guo, G. X. Wang and H. K. Liu, *Electrochim. Acta*, 2005, **51**(1), 23-28.

7 G. Che, B. B. Lakshmi, E. R. Fisher and C. R. Martin, *Nature*, 1998, **393**(6683), 346-349.

8 S. L. Chou, Y. Zhao, J. Z. Wang, Z. X. Chen, H. K. Liu and S. X. Dou, *J. Phys. Chem. C*, 2010, **114**(37), 15862-15867.

9 S. Y. Chew, S. H. Ng, J. Z. Wang, P. Novak, F. Krumeich, S. L. Chou, J. Chen and H. K. Liu, *Carbon*, 2009, **47**(13), 2976-2983.

10 C. Wang, D. Li, C. O. Too and G. G. Wallace, *Chem. Mater.*, 2009, **21**(13), 2604-2606.

11 C. Yuan, L. Yang, L. Hou, J. Li, Y. Sun, X. Zhang, L. Shen, X. Lu, S. Xiong and X. W. Lou, *Adv. Funct. Mater.*, 2012, **22**(12), 2560-2566.

12 H. Gwon, H.-S. Kim, K. U. Lee, D.-H. Seo, Y. C. Park, Y.-S. Lee, B. T. Ahn and K. Kang, *Energy Environ. Sci.*, 2011, **4**(4), 1277-1283.

13 M. Sathiya, A. S. Prakash, K. Ramesha, J. M. Tarascon and A. K. Shukla, *J. Am. Chem. Soc.*, 2011, **133**(40), 16291-16299.

14 H. B. Wu, J. S. Chen, H. H. Hng and X. Wen Lou, *Nanoscale*, 2012, **4**(8), 2526-2542.

15 G. Du, N. Sharma, V. K. Peterson, J. A. Kimpton, D. Jia and Z. Guo, *Adv. Funct. Mater.*, 2011, **21**(20), 3990-3997.

16 Z. Zheng, H. Liu, J. Ye, J. Zhao, E. R. Waclawik and H. Zhu, *J. Mol. Catal. A: Chem.*, 2010, **316**(1–2), 75-82.

17 H. B. Wu, H. H. Hng and X. W. Lou, *Adv. Mater.*, 2012, **24**(19), 2567-2571.

18 D.-H. Kim, Y.-S. Kim, J. Wu, Z. Liu, J. Song, H.-S. Kim, Y. Y. Huang, K.-C. Hwang and J. A. Rogers, *Adv. Mater.*, 2009, **21**(36), 3703-3707.

19 L. Hu, D. S. Hecht and G. Grüner, *Nano Lett.*, 2004, **4**(12), 2513-2517.

20 B. J. Landi, M. J. Ganter, C. D. Cress, R. A. DiLeo and R. P. Raffaelle, *Energy Environ. Sci.*, 2009, **2**(6), 638-654.

21 K. H. Seng, J. Liu, Z. P. Guo, Z. X. Chen, D. Jia and H. K. Liu, *Electrochem. Commun.*, 2011, **13**(5), 383-386.

22 Y. Zhao, Y. Hu, Y. Li, H. Zhang, S. W. Zhang, L. T. Qu, G. Q. Shi and L. M. Dai, *Nanotechnology*, 2010, **21**(50), 505702.

23 C. Jiang, M. Wei, Z. Qi, T. Kudo, I. Honma and H. Zhou, *J. Power Sources*, 2007, **166**(1), 239-243.

24 Y. Wang, H. Liu, K. Wang, H. Eiji, Y. Wang and H. Zhou, *J. Mater. Chem.*, 2009, **19**(37), 6789-6795.